Constraints on the inner edge of neutron star crusts from relativistic nuclear energy density functionals

Moustakidis, Ch. C.; Nikšić, Tamara; Lalazissis, G. A.; Vretenar, Dario; Ring, Peter

Source / Izvornik: **Physical Review C - Nuclear Physics, 2010, 81**

Journal article, Published version
Rad u časopisu, Objavljena verzija rada (izdavačev PDF)

https://doi.org/10.1103/PhysRevC.81.065803

Permanent link / Trajna poveznica: https://urn.nsk.hr/urn:nbn:hr:217:870508

Constraints on the inner edge of neutron star crusts from relativistic nuclear energy density functionals

Ch. C. Moustakidis,[1] T. Nikšić,[2] G. A. Lalazissis,[1] D. Vretenar,[2,3] and P. Ring[3]
[1]*Department of Theoretical Physics, Aristotle University of Thessaloniki, GR-54124 Thessaloniki, Greece*
[2]*Physics Department, Faculty of Science, University of Zagreb, HR-10000 Zagreb, Croatia*
[3]*Physik-Department der Technischen Universität München, D-85748 Garching, Germany*
(Received 21 April 2010; published 28 June 2010)

The transition density n_t and pressure P_t at the inner edge between the liquid core and the solid crust of a neutron star are analyzed using the thermodynamical method and the framework of relativistic nuclear energy density functionals. Starting from a functional that has been carefully adjusted to experimental binding energies of finite nuclei, and varying the density dependence of the corresponding symmetry energy within the limits determined by isovector properties of finite nuclei, we estimate the constraints on the core-crust transition density and pressure of neutron stars: $0.086\ \text{fm}^{-3} \leqslant n_t < 0.090\ \text{fm}^{-3}$ and $0.3\ \text{MeV fm}^{-3} < P_t \leqslant 0.76\ \text{MeV fm}^{-3}$.

DOI: 10.1103/PhysRevC.81.065803 PACS number(s): 26.60.Gj, 21.30.Fe, 21.60.Jz, 26.60.Kp

I. INTRODUCTION

Neutron stars are extraordinary astronomical laboratories for the physics of dense neutron-rich nuclear matter [1,2]. They consist of several distinct layers: the atmosphere, the surface, the crust, and the core. The latter, divided into the outer core and the inner core, has a radius of approximately 10 km and contains most of the star's mass. The crust, of ≈1 km in thickness and containing only a few percent of the total mass, can also be divided into the outer crust and the inner crust. Although less exotic and smaller in size than the core, the crust is nevertheless crucial for the understanding of the physics of neutron stars. It represents the interface between the observable surface phenomena and the invisible core. The structure of the crust can be related to some peculiar phenomena, such as pulsar glitches, thermal relaxation after matter accretion, quasiperiodic oscillations, and anisotropic surface cooling [3–5]. A very important ingredient in the study of the structure and various properties of neutron stars is the equation of state (EOS) of neutron-rich nuclear matter [6].

One of the most important predictions of a given EOS is the location of the inner edge of a neutron star crust. The inner crust is composed of the region from the density at which neutrons drip out of nuclei to the inner edge separating the solid crust from the homogeneous liquid core. At the inner edge, in fact, a phase transition occurs from the high-density homogeneous matter to the inhomogeneous matter at lower densities. In the transitional region nuclear matter exhibits instability against clusterization into a two-phase system: neutron-rich nuclei immersed in dripped neutrons (and sometimes protons). Because nuclei are arranged in a lattice, they form a solid state crust covering the star's core, which is considered to be a homogeneous liquid [7]. The uniform matter is nearly pure neutron matter, with a proton fraction of a few percent, determined by the condition of β equilibrium. The transition density takes its critical value n_c when the uniform neutron-proton-electron matter (npe) becomes unstable with respect to the separation into two coexisting phases (one corresponding to nuclei, the other to a nucleonic sea) [6].

While the density at which neutrons drip out of nuclei is rather well determined, the transition density n_t at the inner edge is much less certain due to our insufficient knowledge of the EOS of neutron-rich nuclear matter. The value of n_t determines the structure of the inner part of the crust. If sufficiently high, it is possible for nonspherical phases, with rod- or platelike nuclei, to occur before the nuclei dissolve. If n_t is relatively low, then matter makes a direct transition from spherical nuclei to uniform nucleonic fluid. The extent to which nonspherical phases occur will have important consequences for other properties that are determined by the solid crust [8].

In general, the determination of the transition density n_t itself is a very complicated problem because the inner crust may have a very complicated structure. A well-established approach is to find the density at which the uniform liquid first becomes unstable against small-amplitude density fluctuations, indicating the formation of nuclear clusters. This approach includes the dynamical method [8–16], the thermodynamical method [6,7,17,18], and the random-phase approximation (RPA) [19,20].

All theoretical studies have shown that the core-crust transition density and pressure are very sensitive to the density dependence of the nuclear matter symmetry energy. The EOS of neutron-rich nuclear matter has been constrained by using results from heavy-ion reaction studies [21]. In particular, it has been shown that the $E_{\text{sym}}(n)$ constrained in the same subsaturation density range as the neutron star crust by the isospin diffusion data in heavy-ion collisions at intermediate energies [22–24] limits the transition density and pressure to $0.040\ \text{fm}^{-3} \leqslant n_t \leqslant 0.065\ \text{fm}^{-3}$ and $0.01\ \text{MeV fm}^{-3} \leqslant P_t \leqslant 0.26\ \text{MeV fm}^{-3}$, respectively. These constrained values appear to be significantly lower than their fiducial values currently used in the literature. In a very recent study [16], the core-crust transition density and pressure have been systematically analyzed using the dynamical and thermodynamical methods with a modified Gogny interaction and a set of 51 different Skyrme interactions. Most of these interactions predict values for the transition density and pressure that are considerably higher than the intervals cited previously.

In a recent work [25] we have explored a particular class of empirical relativistic nuclear energy density functionals, with parameters adjusted to experimental binding energies of a large set of axially deformed nuclei. Starting from microscopic

nucleon self-energies in nuclear matter and empirical global properties of the nuclear matter equation of state, the coupling parameters of the functional have been determined in a careful comparison of the predicted binding energies with data, for a set of 64 axially deformed nuclei in the mass regions $A \approx 150$–180 and $A \approx 230$–250. The isovector channel, in particular, has been carefully adjusted to reproduce available data in medium-heavy and heavy nuclei, including neutron-skin thickness and excitation energies of isovector dipole resonances. It will be interesting, therefore, to apply this class of relativistic density functionals in a systematic investigation of the transition density n_t and pressure P_t at the inner edge separating the liquid core from the solid crust of neutron stars. In the present study a thermodynamical method is used.

In recent years, there has been an increased interest in studies of the relationship between the size of the neutron-skin in heavy nuclei and the symmetry energy at subsaturation densities [19,26–36]. Studies have also been reported on the correlation between the size of the neutron-skin and properties of a neutron star crust. This was pioneered by Horowitz and Piekarewicz [19], who used the RPA based on the relativistic mean-field (RMF) framework for nuclear matter and finite nuclei. An almost linear correlation was established between the predicted core-crust transition density n_t and the size of the neutron skin. More recently such studies have been carried out by Xu *et al.* [15,16], confirming this linear correlation.

This article is organized as follows. In Sec. II we review the thermodynamical method used for locating the inner edge of a neutron star crust. Section III contains a brief description of the relativistic density functionals that are used to analyze the constraints on the core-crust transition density and pressure of neutron stars. The results are presented and discussed in Sec. IV, and Sec. V summarizes the present study.

II. THE THERMODYNAMICAL METHOD

The core-crust interface corresponds to the phase transition between nuclei and uniform nuclear matter. The uniform matter is nearly pure neutron matter, with a proton fraction of just a few percent determined by the condition of β equilibrium. Weak interactions conserve both baryon number and charge [6], and from the first low of thermodynamics, at temperature $T = 0$ (for details see the Appendix),

$$du = -Pdv - \hat{\mu}dq, \tag{1}$$

where u is the internal energy per baryon, P is the total pressure, v is the volume per baryon ($v = 1/n$, where n is the baryon density), and q is the charge fraction ($q = x - Y_e$, where x and Y_e are the proton and electron fraction in baryonic matter, respectively). In β equilibrium the chemical potential $\hat{\mu}$ is given by $\hat{\mu} = \mu_n - \mu_p = \mu_e$, where μ_i is the chemical potential of the protons, neutrons, and electrons. The stability of the uniform phase requires that $u(v, q)$ is a convex function [37]. This condition leads to the following two constraints for the pressure and the chemical potential

$$-\left(\frac{\partial P}{\partial v}\right)_q - \left(\frac{\partial P}{\partial q}\right)_v \left(\frac{\partial q}{\partial v}\right)_{\hat{\mu}} > 0, \tag{2}$$

$$-\left(\frac{\partial \mu}{\partial q}\right)_v > 0. \tag{3}$$

It is assumed that the total internal energy per baryon $u(v, q)$ can be decomposed into baryon (E_N) and electron (E_e) contributions:

$$u(v, q) = E_N(v, q) + E_e(v, q). \tag{4}$$

In this work the well-know parabolic approximation is used for the baryon energy $E_N(v, q)$,

$$E_N(v, q) \simeq V(v) + E_{\rm sym}(v)(1 - 2x)^2, \tag{5}$$

where higher-order terms in the isospin asymmetry $\delta = 1 - 2x$ are neglected. In Eq. (5), $V(v)$ denotes the energy of symmetric nuclear matter, and $E_{\rm sym}(v)$ is given by

$$E_{\rm sym}(v) \simeq E_N[v, q(x = 0)] - E_N[v, q(x = 0.5)]. \tag{6}$$

The electron contribution to the total energy reads

$$E_e = \tfrac{3}{4} Y_e \mu_e. \tag{7}$$

The condition of β equilibrium leads to the relation [38,39]

$$\hat{\mu} = -\left(\frac{\partial E_N}{\partial x}\right)_n = 4E_{\rm sym}(n)(1 - 2x) = \hbar c(3\pi^2 n_e)^{1/3}. \tag{8}$$

From the relation

$$q = x - Y_e = x - n_e/n, \quad n_e = \frac{\mu_e^3}{\hbar^3 c^3 3\pi^2} = \frac{\hat{\mu}^3}{\hbar^3 c^3 3\pi^2}, \tag{9}$$

and Eq. (A16), it follows that

$$\begin{aligned} -\left(\frac{\partial q}{\partial \hat{\mu}}\right)_{v(n)} &= -\left(\frac{\partial x}{\partial \hat{\mu}}\right)_{v(n)} + \frac{1}{n}\left(\frac{\partial n_e}{\partial \hat{\mu}}\right)_{v(n)} \\ &= \frac{1}{8E_{\rm sym}(n)} + \frac{\hat{\mu}^2}{n\hbar^3 c^3 \pi^2} = \frac{1}{8E_{\rm sym}(n)} + \frac{3Y_e}{\hat{\mu}}. \end{aligned} \tag{10}$$

The inequality (2) is equivalent to

$$-\left(\frac{\partial P}{\partial v}\right)_{\hat{\mu}} > 0. \tag{11}$$

The electron contribution to the pressure P_e is a function of the chemical potential $\hat{\mu} = \mu_e$ only

$$P_e = \frac{1}{12\pi^2}\frac{\mu_e^4}{(\hbar c)^3}, \tag{12}$$

and thus the inequality (11) can be written as

$$-\left(\frac{\partial P_b}{\partial v}\right)_{\hat{\mu}} > 0, \quad \text{or} \quad n^2\left(\frac{\partial P_b}{\partial n}\right)_{\hat{\mu}} > 0. \tag{13}$$

In general the baryonic pressure P_b is a function of both n and x, but for a fixed $\hat{\mu}$ [see also Eq. (A16)] $x = x(n)$, so that $P = P[n, x(n)]$, and therefore

$$n^2\left(\frac{\partial P_b}{\partial n}\right)_{\hat{\mu}} = n^2\left[\frac{dP_b}{dn} + \frac{\partial P_b}{\partial x}\left(\frac{\partial x}{\partial n}\right)_{\hat{\mu}}\right]. \tag{14}$$

Now, considering that $\hat{\mu} = \hat{\mu}(n, x)$, it follows that

$$d\hat{\mu} = \left(\frac{\partial\hat{\mu}}{\partial n}\right)_x dn + \left(\frac{\partial\hat{\mu}}{\partial x}\right)_n dx \Rightarrow \left(\frac{\partial x}{\partial n}\right)_{\hat{\mu}} = -\left(\frac{\partial\hat{\mu}}{\partial n}\right)_x \left(\frac{\partial\hat{\mu}}{\partial x}\right)_n^{-1}, \quad (15)$$

and making use of Eq. (A16), one obtains

$$\left(\frac{\partial x}{\partial n}\right)_{\hat{\mu}} = -\left(\frac{\partial^2 E_N}{\partial n \partial x}\right)\left(\frac{\partial^2 E_N}{\partial x^2}\right)^{-1}. \quad (16)$$

Equation (14), with the help of Eq. (25), now reads

$$n^2\left(\frac{\partial P_b}{\partial n}\right)_{\hat{\mu}} = n^4\left[\frac{2}{n}\frac{dE_N}{dn} + \frac{d^2E_N}{dn^2} - \left(\frac{\partial^2 E_N}{\partial n\partial x}\right)^2\left(\frac{\partial^2 E_N}{\partial x^2}\right)^{-1}\right]. \quad (17)$$

The condition of charge neutrality $q = 0$ requires that $x = Y_e$. This is the case we consider in the present study. After some algebra, it can be shown that the conditions (2) and (3) are equivalent to

$$C_I(n) = n^2\frac{d^2V}{dn^2} + 2n\frac{dV}{dn} + (1-2x)^2\left[n^2\frac{d^2E_{\rm sym}}{dn^2} + 2n\frac{dE_{\rm sym}}{dn} - 2\frac{1}{E_{\rm sym}}\left(n\frac{dE_{\rm sym}}{dn}\right)^2\right] > 0, \quad (18)$$

$$C_{II}(n) = -\left(\frac{\partial q}{\partial\hat{\mu}}\right)_v = \frac{1}{8E_{\rm sym}} + \frac{3Y_e}{\hat{\mu}} > 0. \quad (19)$$

The second inequality (19) is usually valid. The transition density n_t is determined from the first inequality (18). For a given EOS, the quantity $C_I(n)$ is plotted as a function of the baryonic density n, and the equation $C_I(n_t) = 0$ defines the transition density n_t.

A. The quantities L and $K_{\rm sym}$

The density dependence of the nuclear matter symmetry energy can be characterized in terms of a few bulk parameters by expanding it in a Taylor series around the saturation density n_0,

$$E_{\rm sym}(n) = E_{\rm sym}(n_0) + L\left(\frac{n-n_0}{3n_0}\right) + \frac{K_{\rm sym}}{2}\left(\frac{n-n_0}{3n_0}\right)^2 + \mathcal{O}(3)\ldots, \quad (20)$$

where $E_{\rm sym}(n_0) \equiv a_4$ is the value of the symmetry energy at saturation, L is the slope parameter,

$$L = 3n_0\left(\frac{\partial E_{\rm sym}(n)}{\partial n}\right)_{n=n_0}, \quad (21)$$

and the curvature parameter $K_{\rm sym}$ is the isovector correction to the compression modulus

$$K_{\rm sym} = 9n_0^2\left(\frac{\partial^2 E_{\rm sym}(n)}{\partial n^2}\right)_{n=n_0}. \quad (22)$$

The slope parameter L is related to P_0, the pressure from the symmetry energy for pure neutron matter at saturation density [40]. The symmetry pressure P_0 provides the dominant baryonic contribution to the pressure in neutron stars at saturation density. It will be interesting to study the relation between the transition density n_t and L and $K_{\rm sym}$, as well as to examine the correlations between L and $K_{\rm sym}$ and the neutron-skin thickness.

The neutron-skin thickness S of a nucleus is defined as the difference between the root-mean-square radii of neutron $\sqrt{\langle r_n^2\rangle}$ and proton $\sqrt{\langle r_p^2\rangle}$ distributions:

$$S = \sqrt{\langle r_n^2\rangle} - \sqrt{\langle r_p^2\rangle} = R_n - R_p. \quad (23)$$

S is sensitive to the density dependence of the nuclear symmetry energy, particularly the slope parameter L [26,31,32]. More specifically, the slope parameter L has been found to correlate linearly with the neutron-skin thickness of heavy nuclei [19,30,31,34].

B. The pressure at the inner edge of a neutron star crust

The pressure at the inner edge is an important quantity directly related to the crustal fraction of the moment of inertia, which can be measured indirectly from observations of pulsar glitches [6]. The total pressure is decomposed into baryon and lepton contributions,

$$P(n, x) = P_b(n, x) + P_e(n, x), \quad (24)$$

where

$$P_b(n, x) = n^2\frac{dE_N}{dn}, \quad E_N(n, x) = V(n) + (1-2x)^2E_{\rm sym}(n). \quad (25)$$

The baryon pressure P_b, therefore, is given by

$$P_b(n, x) = n^2\left[\frac{dV(n)}{dn} + \frac{dE_{\rm sym}}{dn}(1-2x)^2\right]. \quad (26)$$

The electrons are considered as a noninteracting Fermi gas. Their contribution to the total pressure reads

$$P_e(n, x) = \frac{1}{12\pi^2}\frac{\mu_e^2}{(\hbar c)^3} = \frac{\hbar c}{12\pi^2}(3\pi^2 xn)^{4/3}. \quad (27)$$

For a given symmetry energy $E_{\rm sym}(n)$, Eq. (8) determines the equilibrium proton fraction $x(n)$. A simple algebra leads to

$$x(n) = \tfrac{1}{2} - \tfrac{1}{4}\{[2\beta(\gamma+1)]^{1/3} - [2\beta(\gamma-1)]^{1/3}\}, \quad (28)$$

where

$$\beta(n) = 3\pi^2 n[\hbar c/4E_{\rm sym}(n)]^3, \quad \gamma(n) = \left(1 + \frac{2\beta}{27}\right)^{1/2}.$$

III. RELATIVISTIC ENERGY DENSITY FUNCTIONALS

The framework of nuclear energy density functionals (NEDFs) provides, at present, the most complete microscopic approach to the rich variety of structure phenomena in medium-heavy and heavy complex nuclei, including regions of the nuclide chart far from the valley of β stability. By employing global functionals parametrized by a set of ≈10 coupling

constants, the current generation of EDF-based models has achieved a high level of accuracy in the description of ground states and properties of excited states, exotic unstable nuclei, and even nuclear systems at the nucleon drip lines.

There are important advantages in using relativistic density functionals, that is, functionals with manifest covariance. The most obvious is the natural inclusion of the nucleon spin degree of freedom, and the resulting nuclear spin-orbit potential which emerges automatically with the empirical strength in a covariant formulation. The consistent treatment of large isoscalar, Lorentz scalar, and vector self-energies provides a unique parametrization of time-odd components of the nuclear mean-field, that is, nucleon currents. Recently [25] we have explored a particular class of relativistic NEDFs in which only nucleon degrees of freedom are explicitly used in the construction of effective interaction terms. Short-distance correlations, as well as intermediate and long-range dynamics, are effectively taken into account in the nucleon-density dependence of the strength functionals of second-order contact interactions in an effective Lagrangian.

The basic building blocks are the densities and currents bilinear in the Dirac spinor field ψ of the nucleon: $\bar{\psi}\mathcal{O}_\tau\Gamma\psi$, with $\mathcal{O}_\tau \in \{1, \tau_i\}$ and $\Gamma \in \{1, \gamma_\mu, \gamma_5, \gamma_5\gamma_\mu, \sigma_{\mu\nu}\}$. Here τ_i are the isospin Pauli matrices and Γ generically denotes the Dirac matrices. The nuclear ground-state density and energy are determined by the self-consistent solution of relativistic linear single-nucleon Kohn-Sham equations. To derive those equations it is useful to construct an interaction Lagrangian with four-fermion (contact) interaction terms in the various isospace-space channels: isoscalar-scalar $(\bar{\psi}\psi)^2$, isoscalar-vector $(\bar{\psi}\gamma_\mu\psi)(\bar{\psi}\gamma^\mu\psi)$, isovector-scalar $(\bar{\psi}\vec{\tau}\psi)\cdot(\bar{\psi}\vec{\tau}\psi)$, and isovector-vector $(\bar{\psi}\vec{\tau}\gamma_\mu\psi)\cdot(\bar{\psi}\vec{\tau}\gamma^\mu\psi)$. A general Lagrangian can be written as a power series in the currents $\bar{\psi}\mathcal{O}_\tau\Gamma\psi$ and their derivatives, with higher-order terms representing in-medium many-body correlations. The Lagrangian considered in Ref. [25] includes second-order interaction terms, with many-body correlations (short-distance correlations, as well as intermediate and long-range dynamics), encoded in density-dependent coupling functions:

$$\begin{aligned}\mathcal{L} = {} & \bar{\psi}(i\gamma\cdot\partial - m)\psi \\ & - \frac{1}{2}\alpha_S(\hat{n})(\bar{\psi}\psi)(\bar{\psi}\psi) - \frac{1}{2}\alpha_V(\hat{n})(\bar{\psi}\gamma^\mu\psi)(\bar{\psi}\gamma_\mu\psi) \\ & - \frac{1}{2}\alpha_{TV}(\hat{n})(\bar{\psi}\vec{\tau}\gamma^\mu\psi)(\bar{\psi}\vec{\tau}\gamma_\mu\psi) \\ & - \frac{1}{2}\delta_S(\partial_\nu\bar{\psi}\psi)(\partial^\nu\bar{\psi}\psi) - e\bar{\psi}\gamma\cdot A\frac{(1-\tau_3)}{2}\psi. \end{aligned} \quad (29)$$

In addition to the free-nucleon Lagrangian and the point-coupling interaction terms, when applied to nuclei, the model must include the coupling of the protons to the electromagnetic field. The derivative term in Eq. (29) accounts for leading effects of finite-range interactions that are crucial for a quantitative description of nuclear density distribution, for example, nuclear radii. Equation (29) includes only one isovector term, that is, the isovector-vector interaction because, although the isovector strength has a relatively well-defined value, the distribution between the scalar and vector channels is not determined by ground-state data.

The strength and density dependence of the interaction terms of the Lagrangian Eq. (29) are parametrized as follows:

$$\begin{aligned}\alpha_S(n) &= a_S + (b_S + c_S x)e^{-d_S x}, \\ \alpha_V(n) &= a_V + b_V e^{-d_V x}, \\ \alpha_{TV}(n) &= b_{TV} e^{-d_{TV} x}, \end{aligned} \quad (30)$$

where $x = n/n_0$ and n_0 denotes the nucleon density at saturation in symmetric nuclear matter. The set of ten parameters has been adjusted in a multistep parameter fit exclusively to the experimental masses of 64 axially deformed nuclei in the mass regions $A \approx 150$–180 and $A \approx 230$–250. The resulting best-fit functional DD-PC1 has been further tested in calculations of binding energies, charge radii, deformation parameters, neutron-skin thickness, and excitation energies of giant monopole and dipole resonances. The nuclear matter equation of state, corresponding to DD-PC1, is characterized by the following properties at the saturation point: nucleon density $n_0 = 0.152$ fm^{-3}, volume energy $a_v = -16.06$ MeV, symmetry energy $a_4 = 33$ MeV, and the nuclear matter compression modulus $K_{\rm nm} = 230$ MeV.

IV. RESULTS AND DISCUSSIONS

To adjust the functional DD-PC1, in Ref. [25] sets of effective interactions with different values of the volume a_v, surface a_s, and symmetry energy a_4 in nuclear matter were generated, and the corresponding binding energies of deformed nuclei with $A \approx 150$–180 and $A \approx 230$–250 were analyzed. The nuclear matter saturation density, the Dirac mass, and the compression modulus were kept fixed: $n_0 = 0.152$ fm^{-3} in accordance with values predicted by most modern relativistic mean-field models, $m^*_D = 0.58m$ in the narrow interval of values allowed by the empirical energy spacings between spin-orbit partner states in finite nuclei, and $K_{\rm nm} = 230$ MeV to reproduce experimental excitation energies of isoscalar giant monopole resonances in relativistic (Q)RPA calculations.

Nuclear structure data do not constrain the nuclear matter EOS at high nucleon densities. Therefore, two additional points on the $E(n)$ curve in symmetric matter were fixed to the microscopic EOS of Akmal, Pandharipande, and Ravenhall [41], based on the Argonne V_{18} NN potential and the UIX three-nucleon interaction. This EOS has extensively been used in studies of high-density nucleon matter and neutron stars. At almost 4 times nuclear matter saturation density, the point $n = 0.56$ fm^{-3} with $E/A = 34.39$ MeV was chosen and, to have an overall consistency, one point at low density: $n = 0.04$ fm^{-3} with $E/A = -6.48$ MeV (cf. Table VI of Ref. [41]).

The calculated binding energies of finite nuclei are very sensitive to the choice of the nuclear matter volume energy coefficient a_v. In fact, one of the important results of the analysis of deviations between calculated and experimental masses (mass residuals) of Ref. [25] is the pronounced isospin and mass dependence of the residuals on the nuclear matter volume energy at saturation. To reduce the absolute mass residuals to less than 1 MeV and to contain their mass and isotopic dependence, a_v had to be constrained to a

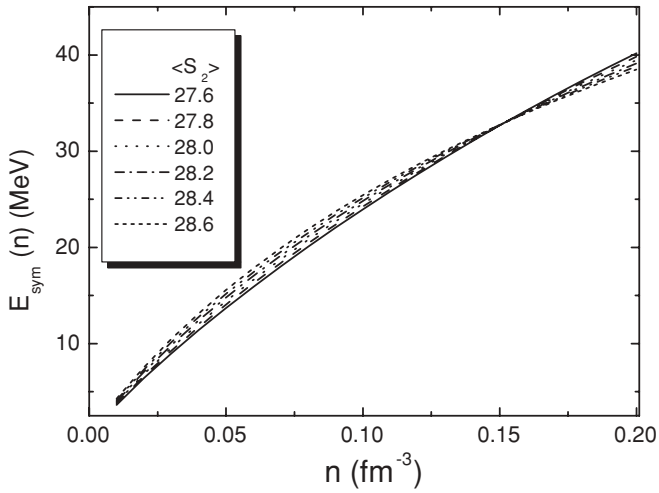

FIG. 1. The symmetry energy $E_{\rm sym}$ as a function of the nucleon density n for various values of the parameter $\langle S_2\rangle$. The symmetry energy at saturation is $a_4 = 33$ MeV.

narrow interval of values: $-16.04\ \text{MeV} \leqslant a_v \leqslant -16.08\ \text{MeV}$. Experimental masses do not place very strict constraints on the parameters of the expansion of $E_{\rm sym}(n)$ [cf. Eq. (20)], but self-consistent mean-field calculations show that binding energies can restrict the values of $E_{\rm sym}$ at nucleon densities somewhat below saturation density, that is, at $n \approx 0.1$ fm^{-3}. Additional information on the symmetry energy can be obtained from data on neutron-skin thickness and excitation energies of giant dipole resonances. Recent studies have shown that relativistic effective interactions with volume asymmetry a_4 in the range $31\ \text{MeV} \leqslant a_4 \leqslant 35$ MeV predict values for neutron-skin thickness that are consistent with data and reproduce experimental excitation energies of isovector giant dipole resonance [42]. Therefore, in the construction of the functional DD-PC1 in Ref. [25], the volume asymmetry was held fixed at $a_4 = 33$ MeV and the symmetry energy at a density that corresponds to an average nucleon density

TABLE I. The values of the transition density n_t (in fm^{-3}) and transition pressure P_t (in Mev fm^{-3}), calculated in the thermodynamical model, as functions of $\langle S_2\rangle$, for $a_4 = 33$ MeV and three values of the nuclear matter volume energy coefficient a_v.

$\langle S_2\rangle$	$a_v = -16.02$ MeV		$a_v = -16.08$ MeV		$a_v = -16.14$ MeV	
	n_t	P_t	n_t	P_t	n_t	P_t
27.6	0.0868	0.598	0.0867	0.590	0.0867	0.592
27.8	0.0870	0.581	0.0869	0.573	0.0869	0.576
28.0	0.0872	0.563	0.0871	0.556	0.0872	0.558
28.2	0.0875	0.544	0.0874	0.537	0.0874	0.539
28.4	0.0878	0.524	0.0877	0.516	0.0877	0.519
28.6	0.0881	0.502	0.0880	0.495	0.0880	0.498

in finite nuclei: $\langle n\rangle = 0.12$ fm^{-3} was varied. The quantity $E_{\rm sym}(n = 0.12\ \text{fm}^{-3})$ is denoted $\langle S_2\rangle$.

Starting from the relativistic energy density functional DD-PC1, in this work we examine the sensitivity of the core-crust transition density n_t and pressure P_t of neutron stars on the density dependence of the corresponding symmetry energy of nucleonic matter. In Ref. [25] the value of $\langle S_2\rangle$ was varied in a rather narrow interval of values $27.6\ \text{MeV} \leqslant \langle S_2\rangle \leqslant 28.6$ MeV, constrained by the empirical values of binding energies and ground-state isovector properties of finite nuclei. Figure 1 displays the corresponding symmetry energy curves $E_{\rm sym}$ as a function of the baryon density n. For $a_v = -16.06$ MeV (DD-PC1) the minimum χ^2 deviation of the theoretical binding energies from data is obtained when $\langle S_2\rangle = 27.8$ MeV.

Table I and Fig. 2 display the values of the transition density n_t (in fm^{-3}) and transition pressure P_t (in MeV fm^{-3}), calculated in the thermodynamical model, as functions of $\langle S_2\rangle$ for three values of the nuclear matter volume energy coefficient a_v. For a given value of the parameter a_v, the values of n_t rise with increasing $\langle S_2\rangle$, whereas the opposite is found for the values of P_t. For the considered interval of $\langle S_2\rangle$, however, the changes are small. An increase of 3.5% in $\langle S_2\rangle$ leads

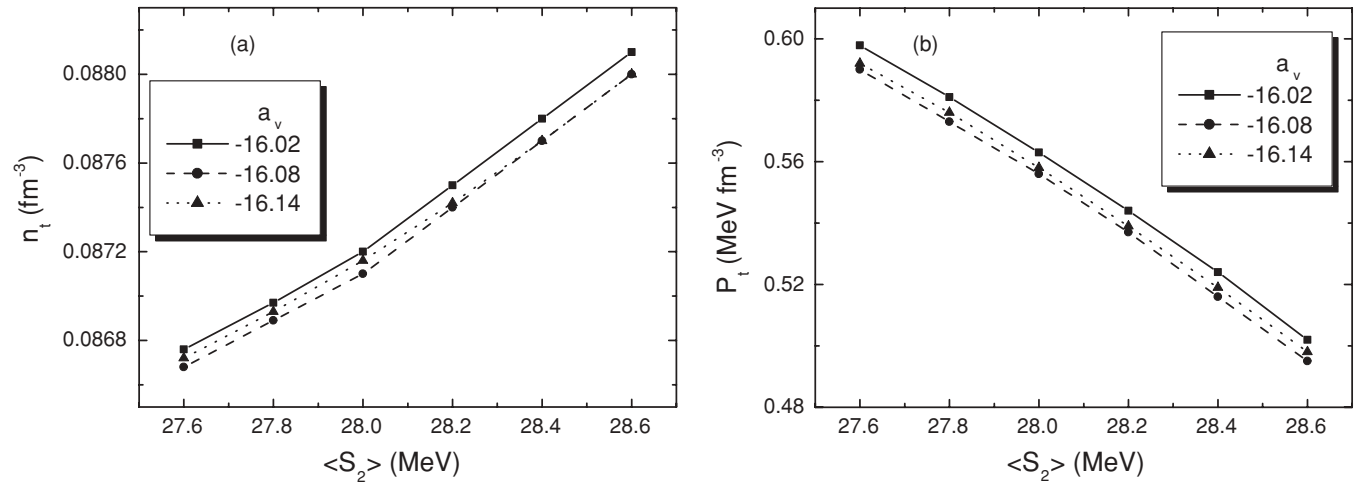

FIG. 2. The transition density n_t (a) and the transition pressure P_t (b), as functions of $\langle S_2\rangle$, for three values of the nuclear matter volume energy coefficient a_v.

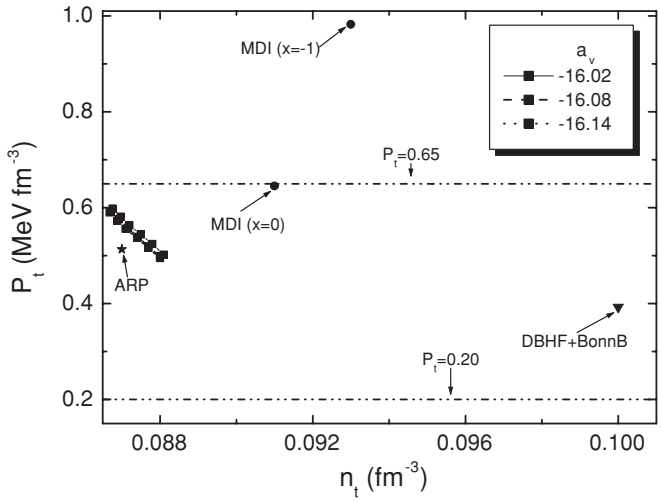

FIG. 3. The transition pressure P_t as a function of the transition density n_t. For a fixed value of the symmetry energy at saturation $a_4 = 33$ MeV and three values of the nuclear matter volume energy coefficient a_v, the parameter $\langle S_2 \rangle$ is varied in the interval between 27.6 and 28.6 MeV. The resulting constraints of P_t and n_t are plotted in comparison with results obtained using different models (for details see Ref. [43]). The lines $P_t = 0.2$ MeV fm^{-3} and $P_t = 0.65$ MeV fm^{-3} correspond to the measure of the current uncertainty in the density dependence of the symmetry energy [6].

to an increase of 1.5% in the value of n_t. The transition pressure exhibits a somewhat more pronounced dependence (the corresponding decrease is around 16% − 20%). Both n_t and P_t display a negligible dependence on a_v, even though $a_v = -16.02$ MeV and $a_v = -16.14$ MeV lie outside the interval of values for which the absolute deviations between calculated and experimental masses are smaller than 1 MeV.

In Fig. 3 we plot the transition pressure P_t as a function of the transition density n_t for the three sets of nuclear matter EOS and symmetry energy described previously, in comparison with results of recent calculations performed using an isospin and momentum-dependent modified Gogny effective interaction (MDI) [16,43]. The different values of the parameter x in the MDI model correspond to various choices of the density dependence of the nuclear symmetry energy. In Refs. [24,44] it has been shown that only $-1 \leqslant x \leqslant 0$ leads to a density dependence of the symmetry energy in the subsaturation density region that is consistent with isospin diffusion data and the empirical value of the neutron-skin thickness in ^{208}Pb. In addition to the MDI EOS, in Fig. 3 we also show the result obtained by Akmal *et al.* [41] with the $A18 + \delta v + UIX^*$ interaction (ARP) and the value obtained in the recent Dirac-Brueckner-Hartree-Fock (DBHF) calculation [32] with the Bonn B One-Boson-Exchange (OBE) potential (DBHF + Bonn B) [45].

A distinctive feature of the present analysis is the narrow interval of allowed values (n_t, P_t) that results from the rather stringent constraints on the parameter $\langle S_2 \rangle$. The effect of varying the volume energy at saturation a_v is almost negligible. The present results for n_t and P_t lie in the region constrained by the measure of the current uncertainty in the density dependence of the symmetry energy [6] and are found very close to the result of Akmal *et al.* [41]. We note that all the results shown in Fig. 3 are obtained using the parabolic approximation for the EOS of isospin-asymmetric nuclear matter. The transition density and pressure have also been estimated using the full equation of state and employing both the dynamical and thermodynamical methods [15,16].

As explained earlier, the rather narrow interval of $\langle S_2 \rangle$, for this type of NEDF, has been constrained by the empirical values of binding energies and ground-state isovector properties of finite nuclei. The symmetry energy at saturation density, $a_4 = 33$ MeV, was fixed in Ref. [25] to obtain the best results for the neutron-skin thickness in Sn isotopes and ^{208}Pb and for the excitation energies of isovector dipole resonances. However, because of large experimental uncertainties, especially for the neutron-skin thickness, good agreement with data can also be obtained for other values of a_4. This is shown in Fig. 4, where we plot the predictions for the differences between neutron and proton rms radii of Sn and Pb isotopes, in comparison with available data [46–48], for different

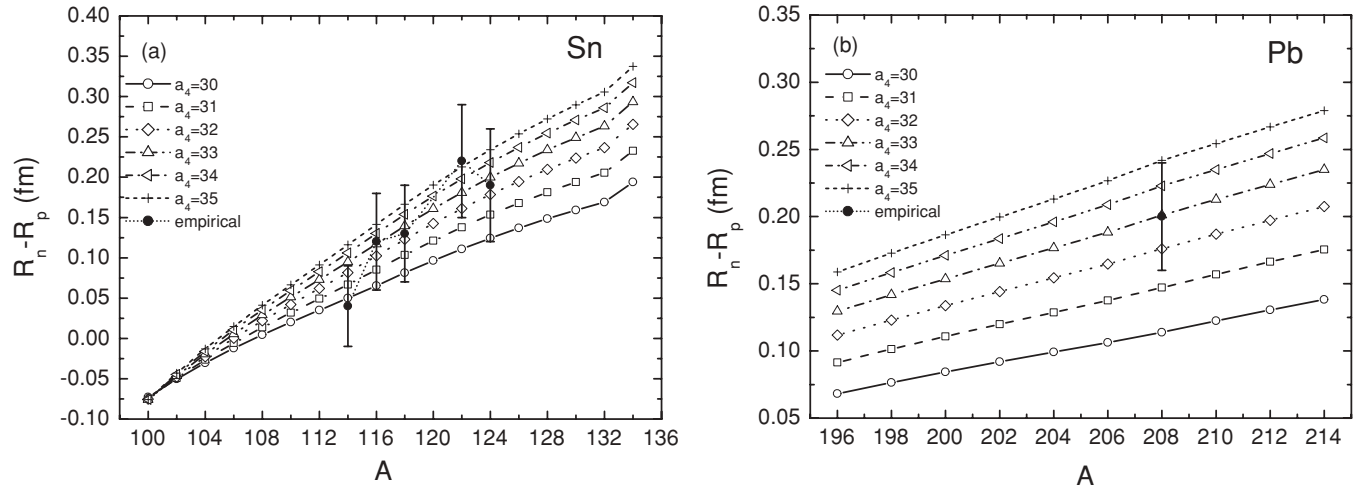

FIG. 4. RHB predictions for the differences between neutron and proton rms radii of (a) Sn and (b) Pb isotopes, in comparison with available data [46–48], for different choices of the symmetry energy at saturation density a_4 (in MeV).

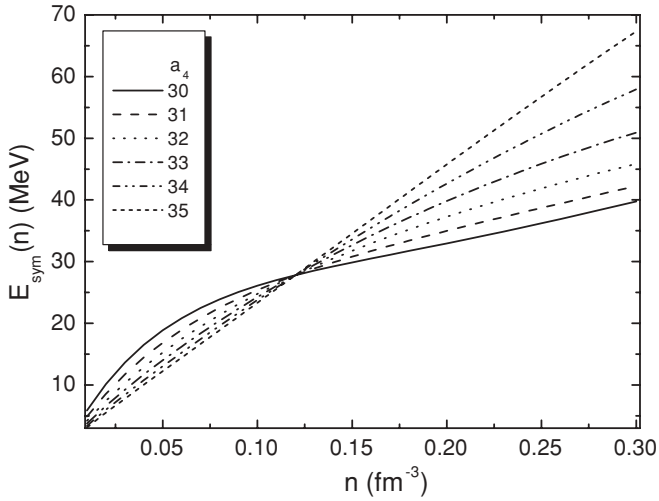

FIG. 5. The symmetry energy $E_{\rm sym}$ as a function of the nucleon density n for various values of the symmetry energy at saturation a_4. The parameter $\langle S_2 \rangle$ (see text) is kept constant at 27.8 MeV.

choices of the symmetry energy at saturation density. The self-consistent mean-field calculations have been performed using the relativistic Hartree-Bogoliubov (RHB) model [49], with pairing correlations described by the pairing part of the finite-range Gogny interaction. The isoscalar channel of the particle-hole interaction corresponds to the DD-PC1 functional, and in the isovector channel $\langle S_2 \rangle$ is kept fixed at 27.8 MeV (DD-PC1), whereas a_4 is varied in the interval between 30 and 35 MeV. The corresponding symmetry energy as a function of the nucleon density is shown in Fig. 5.

We notice, therefore, that by keeping $\langle S_2 \rangle$ constant and varying a_4 in the interval between 30 and 35 MeV, the density dependence of the symmetry energy can be modified in a controlled way, that is, the corresponding energy density functionals still reproduce ground-state properties of finite nuclei in fair agreement with data. In Table II and Fig. 6 we display the corresponding values of the transition density

TABLE II. The values of the transition density n_t (in fm^{-3}) and transition pressure P_t (in Mev fm^{-3}), calculated in the thermodynamical model, as functions of a_4, for $\langle S_2 \rangle = 27.8$ MeV and three values of the nuclear matter volume energy coefficient a_v.

a_4 (MeV)	$a_v =$ −16.02 MeV		$a_v =$ −16.08 MeV		$a_v =$ −16.14 MeV	
	n_t	P_t	n_t	P_t	n_t	P_t
30	0.0922	0.091	0.0921	0.085	0.0921	0.087
31	0.0899	0.303	0.0898	0.297	0.0898	0.299
32	0.0883	0.463	0.0882	0.456	0.0883	0.459
33	0.0873	0.587	0.0872	0.580	0.0873	0.582
34	0.0866	0.682	0.0865	0.675	0.0865	0.677
35	0.0859	0.755	0.0859	0.748	0.0859	0.750

n_t (in fm^{-3}) and transition pressure P_t (in MeV fm^{-3}) as functions of a_4 for three values of the nuclear matter volume energy coefficient a_v. The transition pressure P_t as a function of the transition density n_t for the three sets of nuclear matter EOS and symmetry energy is plotted in Fig. 7. Not surprising, considering the symmetry energy curves of Fig. 5, the constraints on n_t and P_t have been relaxed in this case, and the allowed values span a much larger interval of values compared to the restricted variation of $\langle S_2 \rangle$ shown in Figs. 1 and 2.

To be able to compare the present results for the transition density and transition pressure with recent studies [16], in Fig. 8 we plot the calculated values of n_t and P_t as functions of the slope parameter of the symmetry energy [cf. Eq. (21)] for the two sets of effective interactions described earlier. n_t is a monotonously decreasing and P_t a monotonously increasing function of L. In the small interval of L values determined by the variation of $\langle S_2 \rangle$ between 27.6 and 28.6 MeV, both n_t and P_t display a linear dependence on L. In the much larger interval determined by the variation of a_4 from 30 to 35 MeV, a weak parabolic dependence of n_t and P_t is found. We note that transport model studies of the isospin diffusion data in heavy-ion reactions have constrained the slope parameter L

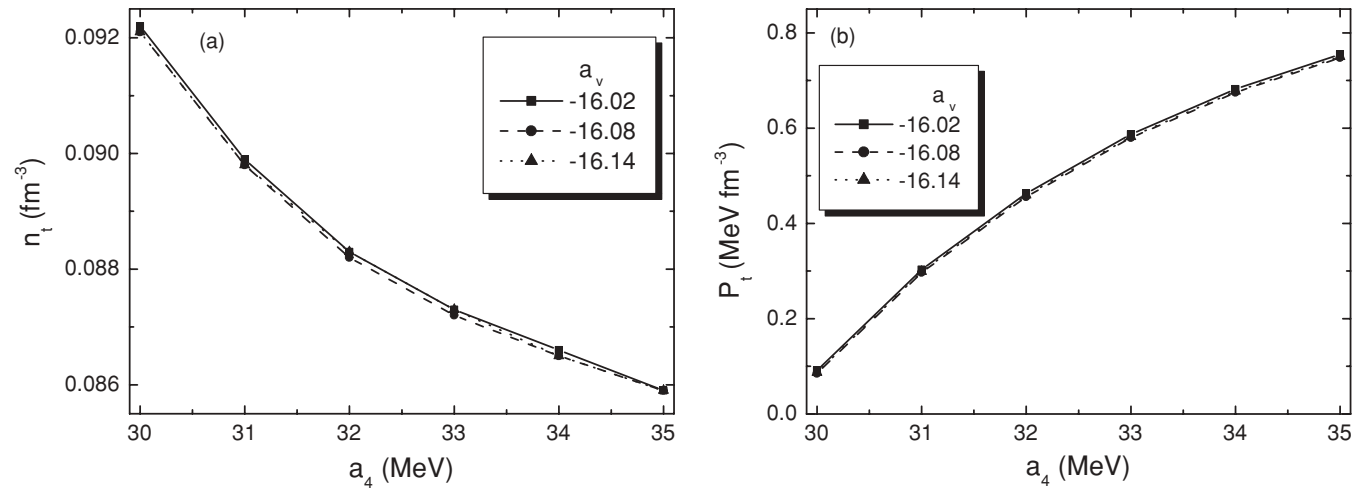

FIG. 6. The transition density n_t (a) and the transition pressure P_t (b), as functions of the symmetry energy at saturation density a_4, for three values of the nuclear matter volume energy coefficient a_v.

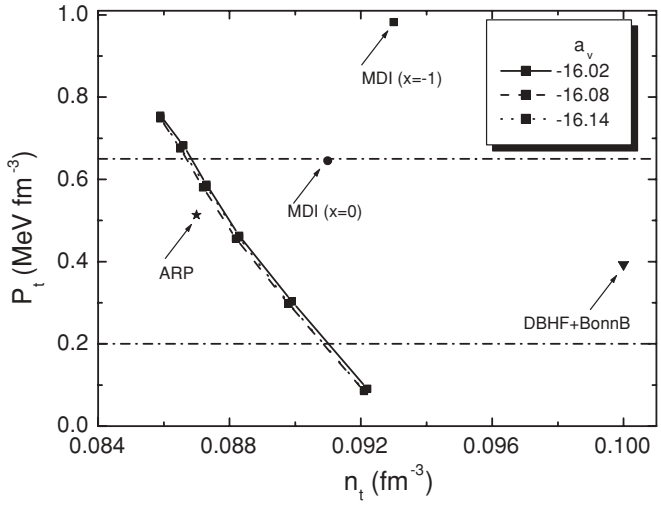

FIG. 7. Same as described in the caption to Fig. 3 but for fixed $\langle S_2 \rangle = 27.8$ MeV and the symmetry energy at saturation in the interval 30 MeV $\leqslant a_4 \leqslant$ 35 MeV.

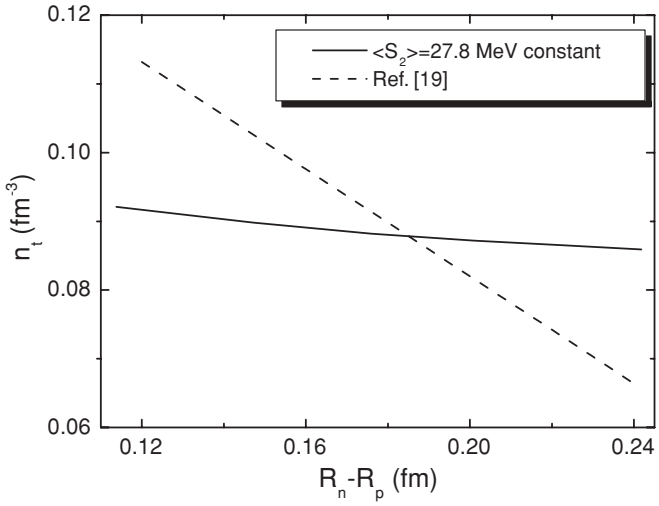

FIG. 9. The transition density n_t as a function of the neutron-skin thickness $R_n - R_p$ of ^{208}Pb. The values of n_t calculated using the thermodynamical model in the present work (solid line) are compared with those of Ref. [19] dashed line (see text for description).

to the values 88 ± 25 MeV [16]. Considering that we can also, most probably, exclude the value $a_4 = 30$ MeV for the asymmetry at saturation density (cf. Figs. 4 and 6), because it implies an unrealistically small value of <0.1 fm for the neutron-skin thickness of ^{208}Pb, the present analysis places the following constraints on the core-crust transition density and pressure of neutron stars: 0.086 fm$^{-3} \leqslant n_t <$ 0.090 fm^{-3} and 0.3 MeV fm$^{-3} < P_t \leqslant$ 0.76 MeV fm^{-3}.

Finally, in Fig. 9 we compare the present prediction for the range of values of the transition density n_t with the results of Horowitz and Piekarewicz who, in Ref. [19], also used the framework of relativistic mean-field effective interactions to study the relationship between the neutron-skin thickness of a heavy nucleus and the properties of neutron star crusts. Starting from the NL3 meson-exchange effective interaction [50], the density dependence of the symmetry energy was varied by adding nonlinear couplings between the isoscalar and isovector mesons to the original interaction. The variation was carried out in such a way to enhance the changes in the neutron density and neutron-skin thickness, while keeping small the corresponding changes in the binding energy and proton density distribution. For the solid crust of a neutron star, the effective RMF interactions were used in a simple RPA calculation of the transition density below which uniform neutron-rich matter becomes unstable against small-amplitude density fluctuations. The resulting transition densities are plotted in Fig. 9 as a function of the predicted difference between neutron and proton rms radii in ^{208}Pb. This inverse correlation was parametrized [19]

$$n_t \approx 0.16 - 0.39(R_n - R_p), \tag{31}$$

with the skin thickness expressed in fm. In the present analysis, using a different type of relativistic effective interaction and varying the density dependence of the symmetry energy by explicitly modifying $\langle S_2 \rangle$ or a_4, we find a much weaker dependence n_t on the neutron-skin thickness of ^{208}Pb.

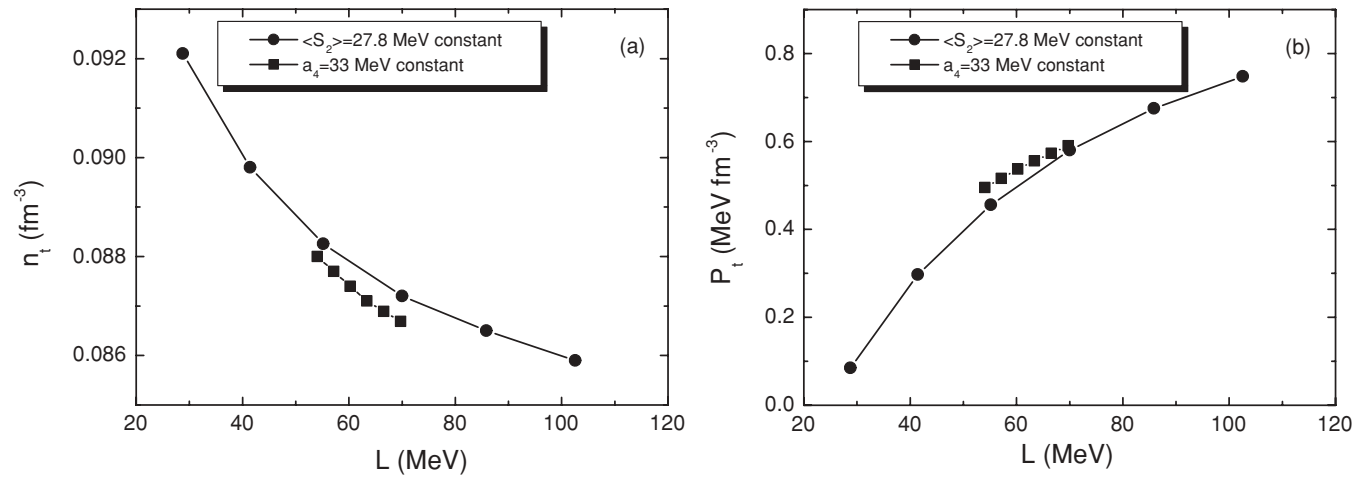

FIG. 8. The transition density n_t (a) and the transition pressure P_t (b) as functions of the slope parameter L.

V. SUMMARY

The framework of relativistic nuclear energy functionals has been employed to analyze and constrain the transition density n_t and pressure P_t at the inner edge between the liquid core and the solid crust of a neutron star, using a thermodynamical method. Starting from a class of energy density functionals carefully adjusted to experimental masses of finite nuclei, we have examined the sensitivity of the core-crust transition density n_t and pressure P_t on the density dependence of corresponding symmetry energy of nucleonic matter. The limits of variation of the density dependence of the symmetry energy are determined by isovector properties of finite nuclei: the thickness of the neutron skin and the excitation energies of isovector giant dipole resonances. Instead of an unrestricted variation of the parameters of the Taylor expansion of the symmetry energy around the saturation density of nuclear matter, that is, the slope parameter and the isovector correction to the compression modulus, we modify the density dependence by varying the value of the nuclear symmetry energy at a point somewhat below the saturation density $\langle S_2 \rangle$ (the symmetry energy at $n = 0.12$ fm^{-3}) and at the saturation density a_4 (the symmetry energy at $n = 0.152$ fm^{-3}, the saturation density for this class of relativistic density functionals). In the former case, for a given value of the volume energy coefficient a_v, $\langle S_2 \rangle$ has been varied in a rather narrow interval of values 27.6 MeV $\leqslant \langle S_2 \rangle \leqslant$ 28.6 MeV determined by a fit to the experimental binding energies. We have found that an increase of 3.5% in $\langle S_2 \rangle$ leads to an increase of 1.5% in the value of n_t while P_t exhibits a somewhat more pronounced dependence (the corresponding decrease is around 16%–20%). Both n_t and P_t display a negligible dependence on a_v. The variation of the parameter a_4 has been in the range of values, 30 MeV $\leqslant a_4 \leqslant$ 35 MeV, allowed by the empirical thickness of the neutron skin and excitation energies of isovector dipole resonances, for a fixed value of $\langle S_2 \rangle$. Again, there is virtually no dependence on a_v, but now both n_t and P_t span much wider intervals. We have also examined the dependence of n_t and P_t on the slope parameter of the symmetry energy L, for the two sets of effective interactions described earlier. For the empirical range of the slope parameter 88 ± 25 MeV, and comparing the calculated values of the neutron-skin thickness with available data for Sn isotopes and ^{208}Pb, we have deduced the following constraints on the core-crust transition density and pressure of neutron stars: 0.086 fm^{-3} $\leqslant n_t <$ 0.090 fm^{-3} and 0.3 MeV fm^{-3} $< P_t \leqslant$ 0.76 MeV fm^{-3}.

The present study will be extended to include also the dynamical and the RPA approaches to analyze the nuclear constraints on the core-crust transition density and pressure of neutron stars. Interesting issues for future study will also be finite temperature and neutrino trapping effects. Work along these lines is in progress.

ACKNOWLEDGMENTS

This work was supported in part by MZOS Project 1191005-1010 and by the DFG cluster of excellence "Origin and Structure of the Universe" (www.universe-cluster.de). T.N. acknowledges support from the Croatian National Foundation for Science. D. Vretenar acknowledges support from the Alexander von Humboldt Foundation.

APPENDIX

A. Proof of the equality $du = -Pdv - \hat{\mu}dq$

From the first low of thermodynamic, at temperature $T = 0$,

$$U = -PdV + \sum_i \mu_i dN_i, \tag{A1}$$

where U is the total energy of $N = \sum_i N_i$ particles in a volume V. Here $i = p, n, e$, and the number of baryons is $N_b = N_n + N_p$. Dividing Eq. (A1) by the baryon number N_b, one obtains

$$u = -Pdv + \sum_i \mu_i dY_i, \tag{A2}$$

with

$$\sum_i \mu_i dY_i = \mu_n \mathrm{Y}_n + \mu_p \mathrm{Y}_p + \mu_e \mathrm{Y}_e \tag{A3}$$

and

$$Y_n = 1 - Y_p. \tag{A4}$$

A simple algebra leads to the following relation:

$$\sum_i \mu_i dY_i = -(\mu_n - \mu_p)dY_p + \mu_e dY_e = -\hat{\mu}dY_p + \hat{\mu}dY_e$$
$$= -\hat{\mu}(dY_p - dY_e) = -\hat{\mu}dq, \tag{A5}$$

where we have used the equalities

$$\hat{\mu} = \mu_n - \mu_p = \mu_e \quad \text{and} \quad q = Y_p - Y_e. \tag{A6}$$

Equation (A2) therefore takes the form

$$du = -Pdv - \hat{\mu}dq. \tag{A7}$$

B. Convexity of the function $u(v, q)$

Let us consider the function $u(v, q)$ and the determinant

$$D = \begin{vmatrix} \frac{\partial^2 u}{\partial v^2} & \frac{\partial u^2}{\partial v \partial q} \\ \frac{\partial u^2}{\partial q \partial v} & \frac{\partial^2 u}{\partial q^2} \end{vmatrix}. \tag{A8}$$

The differential $du(v, q)$ reads

$$du(v, q) = \left(\frac{\partial u}{\partial v}\right)_q dv + \left(\frac{\partial u}{\partial q}\right)_v dq. \tag{A9}$$

From Eqs. (A7) and (A9) it follows that

$$P = -\left(\frac{\partial u}{\partial v}\right)_q, \quad \hat{\mu} = -\left(\frac{\partial u}{\partial q}\right)_v. \tag{A10}$$

The determinant Eq. (A8) takes the form

$$D = \begin{vmatrix} -\left(\frac{\partial P}{\partial v}\right)_q & -\left(\frac{\partial P}{\partial q}\right)_v \\ -\left(\frac{\partial \hat{\mu}}{\partial v}\right)_q & -\left(\frac{\partial \hat{\mu}}{\partial q}\right)_v \end{vmatrix}. \tag{A11}$$

The requirement of convexity for the function $u(v, q)$ leads to the following two sets of inequalities:

Case 1:

$$D > 0, \quad -\left(\frac{\partial P}{\partial v}\right)_q > 0. \tag{A12}$$

Case 2:

$$D > 0, \quad -\left(\frac{\partial \hat{\mu}}{\partial q}\right)_v > 0. \tag{A13}$$

The second set can be written in the form

$$\left(\frac{\partial P}{\partial v}\right)_q \left(\frac{\partial \hat{\mu}}{\partial q}\right)_v - \left(\frac{\partial P}{\partial q}\right)_v \left(\frac{\partial \hat{\mu}}{\partial v}\right)_q > 0, \tag{A14}$$

$$-\left(\frac{\partial \hat{\mu}}{\partial q}\right)_v > 0. \tag{A15}$$

Dividing the inequality (A14) by the positive quantity $-(\frac{\partial \hat{\mu}}{\partial q})_v$, and considering that the differential of the function $\hat{\mu}(v, q)$ is given by

$$d\hat{\mu} = \left(\frac{\partial \hat{\mu}}{\partial v}\right)_q dv + \left(\frac{\partial \hat{\mu}}{\partial q}\right)_v dq, \tag{A16}$$

and therefore for a fixed $\hat{\mu}$

$$\left(\frac{\partial \hat{\mu}}{\partial q}\right)_v = -\left(\frac{\partial \hat{\mu}}{\partial v}\right)_q \left(\frac{\partial q}{\partial v}\right)_{\hat{\mu}}^{-1}, \tag{A17}$$

one obtains the following inequality

$$-\left(\frac{\partial P}{\partial v}\right)_q - \left(\frac{\partial P}{\partial q}\right)_v \left(\frac{\partial q}{\partial v}\right)_{\hat{\mu}} > 0. \tag{A18}$$

[1] S. L. Shapiro and S. A. Teukolsky, *Black Holes, White Dwarfs, and Neutron Stars* (Wiley & Sons, New York, 1983).
[2] P. Haensel, A. Y. Potekhin, and D. G. Yakovlev, *Neutron Stars 1: Equation of State and Structure* (Springer-Verlag, New York, 2007).
[3] J. M. Lattimer and M. Prakash, Phys. Rep. **333-334**, 121 (2000).
[4] J. M. Lattimer and M. Prakash, Astrophys. J. **550**, 426 (2001).
[5] B. Link, R. I. Epstein, and J. M. Lattimer, Phys. Rev. Lett. **83**, 3362 (1999).
[6] J. M. Lattimer and M. Prakash, Phys. Rep. **442**, 109 (2007).
[7] S. Kubis, Phys. Rev. C **76**, 025801 (2007); J. Porebska and S. Kubis, arXiv:0910.5066.
[8] C. J. Pethick, D. G. Ravenhall, and C. P. Lorenz, Nucl. Phys. A **584**, 675 (1995).
[9] G. Baym, C. Pethick, and P. Sutherland, Astrophys. J. **170**, 299 (1971).
[10] G. Baym, H. A. Bethe, and C. J. Pethick, Nucl. Phys. A **175**, 225 (1971).
[11] C. J. Pethick and D. G. Ravenhall, Annu. Rev. Nucl. Part. Sci. **45**, 429 (1995).
[12] F. Douchin and P. Haensel, Phys. Lett. B **485**, 107 (2000).
[13] K. Oyamatsu and K. Iida, Phys. Rev. C **75**, 015801 (2007).
[14] C. Ducoin, Ph. Chomaz, and F. Gulminelli, Nucl. Phys. A **789**, 403 (2007).
[15] J. Xu, L. W. Chen, B. A. Li, and H. R. Ma, Phys. Rev. C **79**, 035802 (2009).
[16] J. Xu, L. W. Chen, B. A. Li, and H. R. Ma, Astrophys. J. **697**, 1549 (2009).
[17] S. Kubis, Phys. Rev. C **70**, 065804 (2004).
[18] A. Worley, P. G. Krastev, and B. A. Li, Astrophys. J. **685**, 390 (2008).
[19] C. J. Horowitz and J. Piekarewicz, Phys. Rev. Lett. **86**, 5647 (2001).
[20] J. Carriere, C. J. Horowitz, and J. Piekarewicz, Astrophys. J. **593**, 463 (2003).
[21] B. A. Li, L. W. Chen, and C. M. Ko, Phys. Rep. **464**, 113 (2008).
[22] M. B. Tsang *et al.*, Phys. Rev. Lett. **92**, 062701 (2004).
[23] L. W. Chen, C. M. Ko, and B. A. Li, Phys. Rev. Lett. **94**, 032701 (2005); Phys. Rev. C **72**, 064309 (2005).
[24] B. A. Li and L. W. Chen, Phys. Rev. C **72**, 064611 (2005).
[25] T. Nikšić, D. Vretenar, and P. Ring, Phys. Rev. C **78**, 034318 (2008).
[26] B. A. Brown, Phys. Rev. Lett. **85**, 5296 (2000).
[27] R. J. Furnstahl, Nucl. Phys. A **706**, 85 (2002).
[28] A. E. L. Dieperink, Y. Dewulf, D. Van Neck, M. Waroquier, and V. Rodin, Phys. Rev. C **68**, 064307 (2003).
[29] A. W. Steiner, M. Prakash, J. M. Lattimer, and P. J. Ellis, Phys. Rep. **411**, 325 (2005).
[30] B. G. Todd-Rutel and J. Piekarewicz, Phys. Rev. Lett. **95**, 122501 (2005).
[31] L. W. Chen, C. M. Ko, and B. A. Li, Phys. Rev. C **72**, 064309 (2005).
[32] F. Sammarruca and P. Liu, Phys. Rev. C **79**, 057301 (2009); F. Sammarruca, arXiv:1002.0146 [nucl-th].
[33] I. Vidana, C. Providencia, A. Polls, and A. Rios, Phys. Rev. C **80**, 045806 (2009).
[34] M. Centelles, X. Roca-Maza, X. Vinas, and M. Warda, Phys. Rev. Lett. **102**, 122502 (2009).
[35] S. Yoshida and H. Sagawa, Phys. Rev. C **69**, 024318 (2004).
[36] A. Klimkiewicz *et al.*, Phys. Rev. C **76**, 051603(R) (2007).
[37] H. B. Callen, *Thermodynamics* (Wiley, New York, 1985).
[38] M. Prakash, *The Equation of State and Neutron Star*, lectures delivered at the Winter School held in Puri India, 1994.
[39] V. P. Psonis, Ch. C. Moustakidis, and S. E. Massen, Mod. Phys. Lett. A **22**, 1233 (2007).
[40] M. B. Tsang, Y. Zhang, P. Danielewicz, M. Famiano, Z. Li, W. G. Lynch, and A. W. Steiner, Phys. Rev. Lett. **102**, 122701 (2009).
[41] A. Akmal, V. R. Pandharipande, and D. G. Ravenhall, Phys. Rev. C **58**, 1804 (1998).
[42] D. Vretenar, T. Nikšić, and P. Ring, Phys. Rev. C **68**, 024310 (2003).
[43] P. G. Krastev and B. A. Li, arXiv:1001.0353 [astro-ph.SR].
[44] B. A. Li and A. W. Steiner, Phys. Lett. B **642**, 436 (2006).
[45] R. Machleidt, Adv. Nucl. Phys. **19**, 189 (1989).
[46] A. Krasznahorkay *et al.*, Phys. Rev. Lett. **82**, 3216 (1999).
[47] V. E. Starodubsky and N. M. Hintz, Phys. Rev. C **49**, 2118 (1994).
[48] A. Krasznahorkay *et al.*, Nucl. Phys. A **567**, 521 (1994).
[49] D. Vretenar, A. V. Afanasjev, G. A. Lalazissis, and P. Ring, Phys. Rep. **409**, 101 (2005).
[50] G. A. Lalazissis, J. König, and P. Ring, Phys. Rev. C **55**, 540 (1997).